Journal of Solid State Chemistry **153,** 254–262 (2000)
doi:10.1006/jssc.2000.8751, available online at http://www.idealibrary.com on IDEAL®

Synthesis, Structural Chemistry, and Magnetic Properties of $Ca_{3.1}Cu_{0.9}RuO_6$

C. A. Moore, E. J. Cussen,[1] and P. D. Battle[2]

Inorganic Chemistry Laboratory, Oxford University, South Parks Road, Oxford OX1 3QR, United Kingdom

Received February 8, 2000; in revised form April 17, 2000; accepted April 20, 2000; published online July 11, 2000

A polycrystalline sample of $Ca_{3.1}Cu_{0.9}RuO_6$ has been synthesized by standard ceramic techniques. The crystal structure, determined at room temperature by neutron powder diffraction, is a monoclinic distortion of the rhombohedral, pseudo one-dimensional K_4CdCl_6 structure: space group $C2/c$, $a = 8.99775(4)$, $b = 9.25809(4)$, $c = 6.47424(2)$ Å, and $\beta = 91.629(1)^\circ$. The octahedrally coordinated cation site is occupied by Ru and the trigonal prismatic site by 10% Ca, 90% Cu. The latter cations are displaced in an ordered manner away from the center of the prism towards one of the rectangular faces; their coordination number is thus reduced to 4. Neutron diffraction data show the onset of long-range magnetic order at 42(2) K. The data suggest collinear ferrimagnetic ordering of the Cu and Ru spins within each chain and antiferromagnetic interchain coupling. However, a small remanent magnetization of 9×10^{-3} μ_B per formula unit was measured by SQUID magnetometry at 5 K. The magnetic structure of $Ca_{3.1}Cu_{0.9}RuO_6$ contrasts with the 120° spin structure adopted by other K_4CdCl_6 phases that do not contain a Jahn–Teller cation; in those cases, the frustration inherent in the lattice is not lifted by a structural distortion.

INTRODUCTION

It is well known that the electronic properties of solids are dependent on the atomic arrangement in the material. In particular, the adoption of a crystal structure containing low-dimensional motifs can lead to unusual electronic behavior, and compounds that adopt such crystal structures are the subject of much contemporary research. The portfolio of one-dimensional compounds chosen for study includes many that are isostructural with K_4CdCl_6 (1), each unit cell of which contains three chains, each composed of alternating chloride octahedra and trigonal prisms as shown in Fig. 1. These polyhedra are occupied by Cd^{2+} and K^+, respectively, and the remaining K^+ cations occupy the spaces between the chains. The resurgence in interest in this long-established structure is, in part, due to the variety of elements that can be introduced into oxide analogues, for example, Sr_3MIrO_6 (M = Ni, Cu, Zn) (2) and S_3MgMO_6 (M = Pt, Ir, Rh) (3). The majority of these phases retain the rhombohedral symmetry of the parent compound, but the introduction of Cu can lead to subtle changes in the crystal structure. Although the structures of the compounds Sr_3IrCuO_6 (4), Ca_3IrCuO_6 (5), and Sr_3PtCuO_6 (6, 7) are similar to that of K_4CdCl_6, with the 5d metal in octahedral coordination and Cu in the trigonal prism, they are modified so as to minimize the electronic energy of the Jahn–Teller active Cu^{2+} cation, which is displaced from the center of the prism towards one of the rectangular faces. This displacement is ordered through the structure and the symmetry of these compositions is thus lowered from rhombohedral to monoclinic.

A wide range of magnetic properties has been observed in this structural family. It is convenient to subdivide the compounds into two groups: those in which magnetic cations are located only in the octahedral sites and those in which the prisms and the octahedra both contain magnetic species. Members of the former, magnetically dilute group generally show evidence of antiferromagnetic coupling with a susceptiblity maximum in the temperature range $10 \leq T/\mathrm{K} \leq 50$ (8–10). This behavior has been interpreted in terms of a one-dimensional Ising model, although it has been pointed out that the superexchange pathways between cations in the same chain are not significantly shorter than those between cations in different chains. Long-range antiferromagnetic ordering has been confirmed by neutron diffraction in relatively few cases, but studies on Ca_3MRuO_6 (M = Li, Na), which contain Ru^{5+} on the octahedral site and the diamagnetic alkali metal in the trigonal prisms, demonstrate (11, 12) that although the structures are apparently one-dimensional, the magnetic properties are typically three-dimensional, with a collinear antiferromagnetic structure being adopted at a Néel temperature $T_N \sim 100$ K. The magnetic dilution of the polyhedral chains by diamagnetic Li^+ or Na^+ clearly results in a weakening of the intrachain interactions to the extent that their strength is

[1]Present address: Chemistry Department, Liverpool University, Liverpool L69 7ZD, U.K.

[2]To whom correspondence should be addressed.

0022-4596/00 $35.00

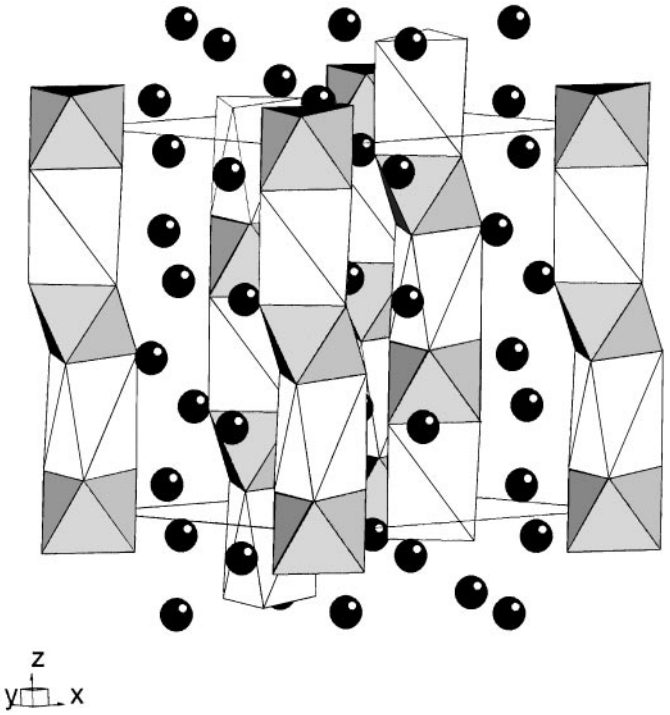

FIG. 1. Crystal structure of K_4CdCl_6 showing [001] chains of $CdCl_6$ octahedra (shaded) and KCl_6 trigonal prisms. Shaded circles represent K atoms in the interchain space.

not significantly greater than that of the interchain interactions. Similar conclusions have been drawn from a study (13) of Ca_3ZnMnO_6, although the Néel temperature of that compound is 25.5 K; it is not obvious why the Néel temperature of the Ru systems is higher than those of the other dilute compounds studied. The magnetically concentrated compound Ca_3NiMnO_6, containing Mn and Ni in the octahedral and trigonal prismatic sites, respectively, orders (13) antiferromagnetically at 20 K, with the magnetic moment in each polyhedron being aligned antiparallel to those in the adjacent polyhedra of the same chain; the moments in neighboring chains are arranged at angles of 120° to each other in a similar manner to that reported for the structurally related compounds $Ba_6Mn_4MO_{15}$ (M = Cu, Zn) (14) and the 2H perovskite halides (15). The adoption of noncollinear spin structures by these materials was ascribed to the frustrated nature of the magnetic sublattice, a complication that is absent in the magnetically dilute compositions.

In this paper we describe the magnetic properties and structure of $Ca_{3.1}Cu_{0.9}RuO_6$. The Ca/Ru/Cu/O system was expected to show a monoclinic distortion, as in the case of Sr_3IrCuO_6, and it was our intention to investigate the effect of this distortion on the magnetic behavior of K_4CdCl_6-like compounds. Moreover, all the magnetically concentrated compounds that have been shown by neutron diffraction to possess a magnetically ordered low-temperature phase have contained exclusively 3*d* metals. The system chosen for study contains a 4*d* element and offers the opportunity to investigate whether the enhanced magnetic transition temperatures observed in dilute compounds of Ru^{5+} can be raised still further in concentrated compounds of Ru^{4+}.

EXPERIMENTAL

Initially, we attempted to prepare the composition Ca_3CuRuO_6, but the reaction product always contained CuO. We concluded that lowering the Cu content might result in a single phase and we subsequently prepared $Ca_{3.1}Cu_{0.9}RuO_6$; attempts to lower the Cu content further took us out of the single-phase regime, which is clearly very narrow. $Ca_{3.1}Cu_{0.9}RuO_6$ was prepared using standard solid-state techniques. Stoichiometric quantities of Alfa (purity, $\geq 99.9\%$) $CaCO_3$, CuO, and RuO_2 (dried) were intimately mixed in an agate mortar and pestle. The mixture was heated overnight at 800°C to decompose the carbonates before being pelleted and fired in an alumina crucible at 800°C for 95 h, 900°C for 19 h, 1000°C for 22 h, and 1100°C for 24 h with intermittent grinding. The progress of the reaction was monitored by X-ray powder diffraction and deemed to be complete when the diffraction pattern did not change upon further heating of the sample.

Time-of-flight neutron diffraction data were collected at room temperature and 4.5 K on the high-resolution powder diffractometer (HRPD) at ISIS, Rutherford Appleton Laboratory, over the d-spacing range $0.7 \leq d/\text{Å} \leq 2.5$. Additional studies were carried out on the low-resolution neutron diffractometer D1b at the Institut Laue-Langevin in Grenoble over a 2θ range of $10° \leq 2\theta \leq 90°$ with a wavelength of 2.531 Å ($1.96 \leq d/\text{Å} \leq 14.5$). Use of this instrument enabled the diffraction pattern to be monitored continuously while heating through the temperature range $1.7 \leq T/\text{K} \leq 81.7$, with the data being summed and stored at temperature intervals of 4 K. Rietveld (16) analysis of the powder X-ray and neutron data was carried out using the GSAS program (17). Magnetic susceptibility measurements were performed using a Quantum Design SQUID magnetometer. The susceptibilities were recorded in fields of 100 and 1000 G after cooling in both zero field (ZFC) and the measuring field (FC). Measurements of magnetization as a function of field were carried out at selected temperatures in the field range $-20 \leq H/\text{kG} \leq 20$. A two-probe conductivity measurement on a sintered pellet at room temperature showed that the sample was insulating with $\rho \sim 10^4$ Ω-cm.

RESULTS

The X-ray diffraction pattern of the reaction product was consistent with the adoption of a distorted K_4CdCl_6 struc-

TABLE 1
Atomic Coordinates of $Ca_{3.1}Cu_{0.9}RuO_6$ at Room Temperature

Atom	Site	x	y	z	U_{iso} (Å^2)
Ca1	4*e*	$\frac{1}{2}$	0.8987(2)	$\frac{1}{4}$	0.0059(6)
Ca2	8*f*	0.6837(1)	0.5757(2)	0.3829(2)	0.0059(4)
Ru	4*c*	$\frac{3}{4}$	$\frac{3}{4}$	0	0.0019(4)
Cu/Ca[a]	4*e*	$\frac{1}{2}$	0.6913(1)	$\frac{3}{4}$	0.0119(5)
O1	8*f*	0.94354(9)	0.15020(9)	0.45335(1)	0.0055(4)
O2	8*f*	0.28015(9)	0.6839(1)	0.7925(1)	0.0060(4)
O3	8*f*	0.35840(9)	0.92782(9)	0.5656(1)	0.0027(4)

[a]90% Cu, 10% Ca; $a = 8.99775(4)$, $b = 9.25809(4)$, $c = 6.47424(2)$ Å, $\beta = 91.629(1)^\circ$, $R_{wp} = 5.31\%$, $\chi^2 = 6.0$.

TABLE 2
Interatomic Distances (Å) and Angles (°) for $Ca_{3.1}Cu_{0.9}RuO_6$ at Room Temperature

Ca1–O1	2.705(2)	×2	Ru–O1	2.002(1)	×2
Ca1–O2	2.641(1)	×2	Ru–O2	2.001(1)	×2
Ca1–O3	2.452(1)	×2	Ru–O3	1.954(1)	×2
Ca1–O3	2.354(1)	×2			
Ca2–O1	2.326(2)		Cu/Ca–O1	2.008(1)	×2
Ca2–O1	2.527(2)		Cu/Ca–O2	2.006(1)	×2
Ca2–O1	2.623(2)		Cu/Ca–O3	2.786(1)	×2
Ca2–O2	2.343(2)				
Ca2–O2	2.682(2)				
Ca2–O2	2.465(2)		shortest O–O	2.695(2)	
Ca2–O3	2.374(2)				
Ca2–O3	2.623(2)				
O1–Cu/Ca–O1	158.2(1)		O1–Ru–O2	84.64(4)	
O1–Cu/Ca–O2	84.33(3)		O1–Ru–O3	90.57(4)	
O1–Cu/Ca–O2	94.94(4)		O2–Ru–O3	90.06(4)	
O2–Cu/Ca–O2	176.15(9)				

ture. ICP emission spectroscopy gave a metal analysis consistent with the composition $Ca_{3.1}Cu_{0.9}RuO_6$: Ca 31.8% (32.8%), Cu 14.9% (15.1%), and Ru 26.8% (26.7%). The room temperature crystal structure was refined by Rietveld analysis of the neutron powder diffraction data. The background levels were fitted by Chebyshev polynomials, and the peak shapes were described by pseudo-Voigt functions. The structure could be refined in the monoclinic space group $C2/c$, with 41 variables (including 14 atomic positions and 7 isotropic temperature factors) being utilized in the final stages of the refinement. $Ca_{3.1}Cu_{0.9}RuO_6$ does thus show the same monoclinic distortion of the K_4CdCl_6 structure as was observed in Sr_3CuIrO_6. The refined structural parameters are given in Table 1 and selected interatomic distances and angles are listed in Table 2. The interchain sites are occupied by Ca1 and Ca2, the octahedral sites by Ru, and the prisms by Ca and Cu in a 1:9 ratio. It was not possible to identify different sites within the prisms for the two different cations, although the magnitude of the thermal parameter suggests that there is likely to be local static disorder around the average Cu/Ca site described in Table 1. The observed and calculated neutron diffraction patterns, and their difference, are shown in Fig. 2 and the structure is drawn in Fig. 3. The chains of alternating RuO_6

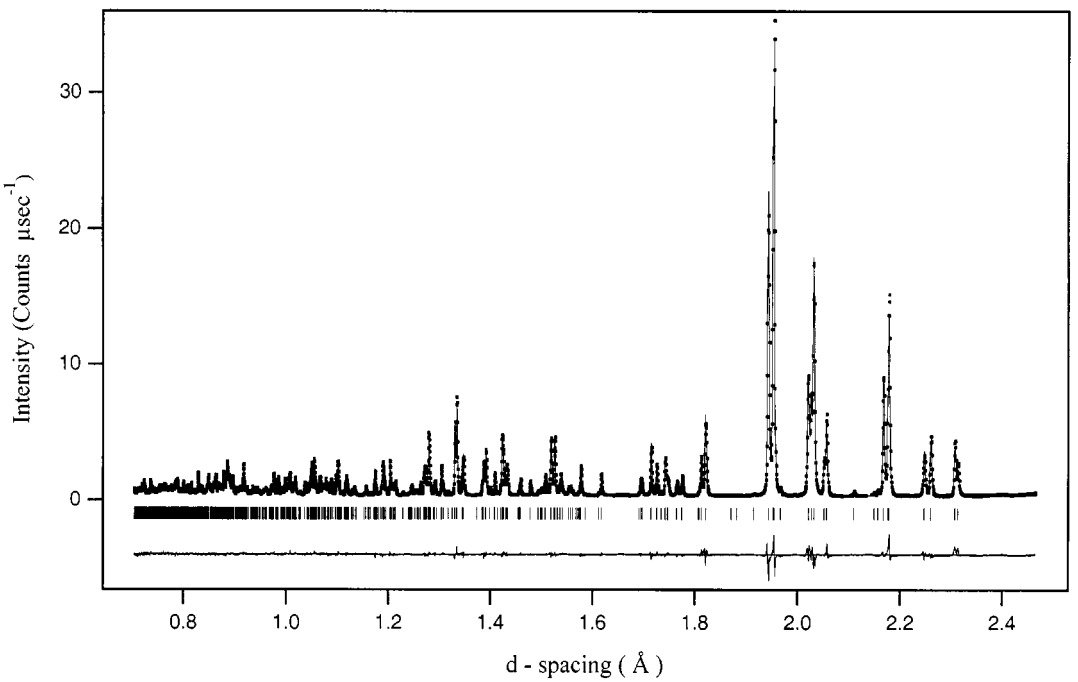

FIG. 2. Observed, calculated, and difference neutron diffraction patterns of $Ca_{3.1}Cu_{0.9}RuO_6$ at room temperature. Reflection positions are marked.

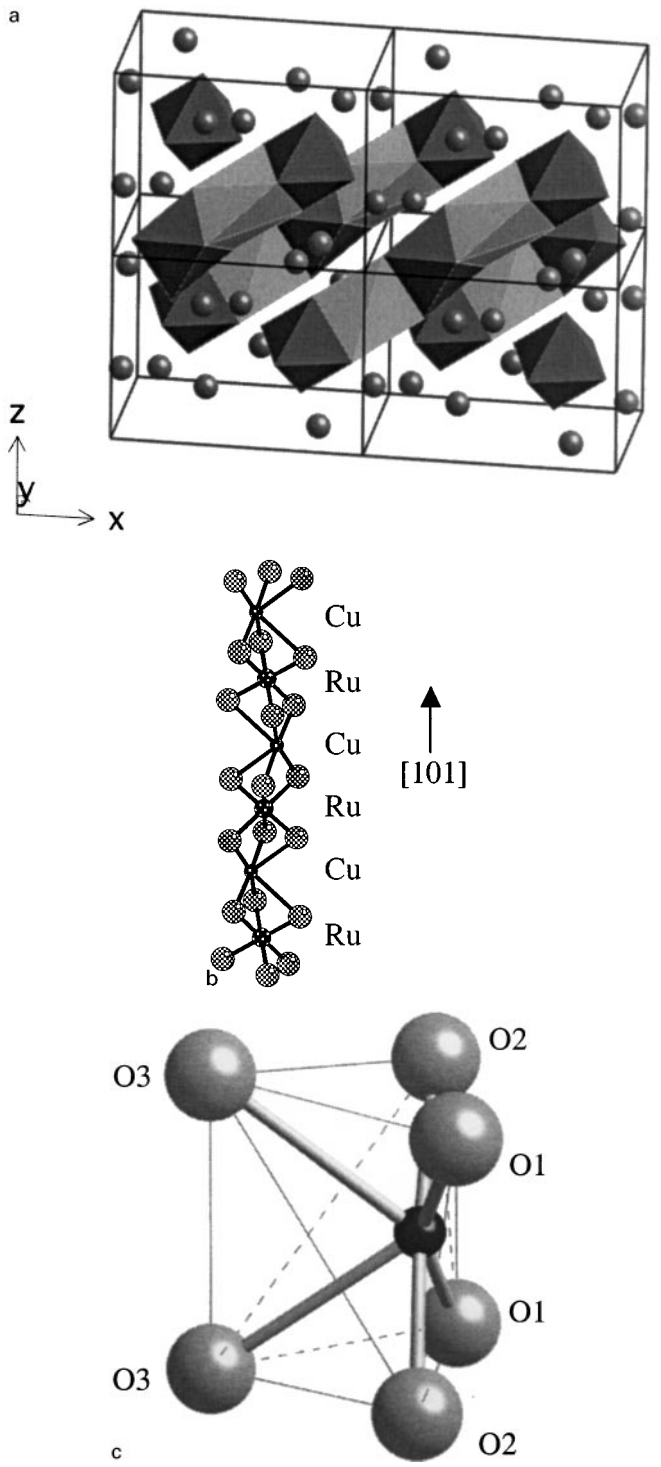

FIG. 3. Crystal structure of $Ca_{3.1}Cu_{0.9}RuO_6$ showing (a) the orientation of the polyhedral chains within the monoclinic unit cell, (b) the atomic arrangement within one chain, and (c) details of the prismatic site.

octahedra and CuO_6 trigonal prisms are aligned along the [101] direction of the monoclinic unit cell.

The molar magnetic susceptibility measured in a field of 1 kG is shown in Fig. 4. The data show a divergence of the FC and ZFC susceptibilities at 53(2) K and a maximum in the ZFC susceptibility at 12(1) K. Fitting the data to the Curie–Weiss Law in the temperature range $150 \leq T/\mathrm{K} \leq 300$ resulted in the parameters $C = 2.497(7)$ emu and $\theta = -343(2)$ K; attempts to include a temperature-independent term in the model did not lead to a significant improvement in the fit nor did the parameters θ and C change significantly. The susceptibility was independent of field in the selected temperature range. The field dependence of the magnetization at 80, 35, and 5 K is plotted in Fig. 5. It can be seen from these data that hysteresis is present at 5 K and, less obviously, at 35 K, but is absent at 80 K. The hysteresis loops are symmetrical about the origin and the remanent magnetization at 5 K corresponds to $\sim 9 \times 10^{-3}\ \mu_B$ per formula unit. Analysis of the neutron diffraction data collected with HRPD at 4.5 K showed that there is no significant change in the atomic coordinates upon cooling, although there is a slight contraction of the lattice parameters (at 4.5 K, $a = 8.98449(5)$, $b = 9.23481(5)$, $c = 6.46014(3)$ Å, $\beta = 91.564(1)^\circ$, $R_{wpr} = 3.86\%$, and $\chi^2 = 5.8$). The diffraction pattern collected on the diffractometer D1b at 3.7 K included five weak peaks at low angles that could be indexed in this unit cell, but which are forbidden by the C-centering symmetry element of space group $C2/c$. These peaks were taken to demonstrate the presence of long-range magnetic order. Several magnetic models were investigated in an attempt to account for the observed distribution of magnetic scattering. Trial models that only allowed a magnetic moment on the octahedral Ru sites or on the trigonal prismatic Cu sites were each considered. These models could not account for the appearance of magnetic peaks at the observed d-spacings. The model that correctly predicts the positions and intensities of the magnetic peaks (Fig. 6) is based on a collinear spin structure, with both the Ru and Cu cations possessing an ordered magnetic moment. These are aligned (Fig. 7) in an antiferromagnetic manner within the chains, resulting in each chain being ferrimagnetic, as the moments of the ruthenium atoms and the copper atoms are not of equal magnitude. The spins are aligned along the $[10\bar{1}]$ direction, which is perpendicular to the direction of the chains, and the interchain coupling is such that the ferrimagnetic contributions sum to zero; the remanent magnetization detected by magnetometry is too weak to be detected by neutron diffraction. In the analysis of the data collected on D1b, all atomic positions were constrained to the values calculated from the 4.5 K HRPD refinement. The magnitudes of the magnetic moments refined to values of 1.1(1) μ_B per Ru and 0.5(1) μ_B per Cu at 3.7 K. Analysis of the diffraction patterns collected while the sample was being warmed (Fig. 8) showed that the intensities of the Bragg peaks characteristic of long-range magnetic ordering decrease smoothly and vanish at 42(2) K, a temperature slightly lower than that at which the ZFC and FC susceptibilities diverge. The weak peak observed at $2\theta \sim 38^\circ$ throughout

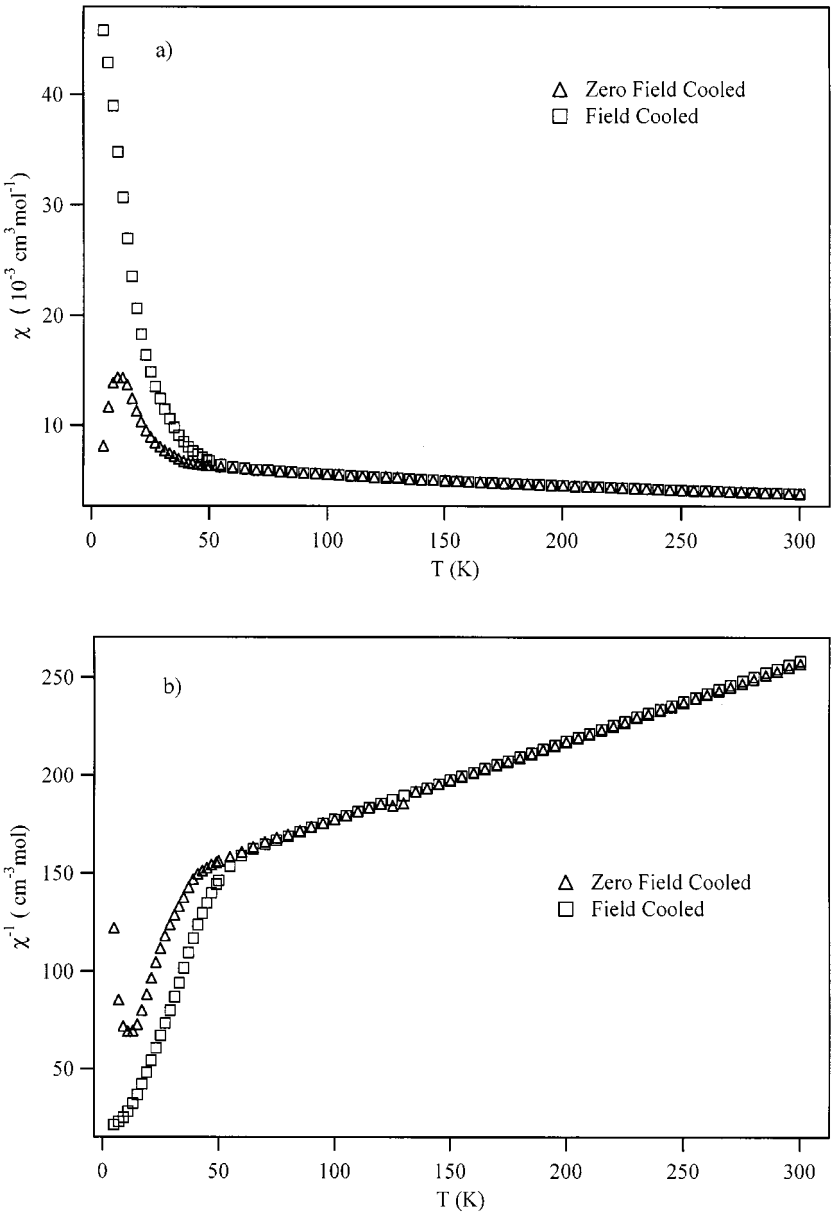

FIG. 4. Temperature dependence of (a) the molar magnetic susceptibility and (b) the inverse molar magnetic susceptibility of $Ca_{3.1}Cu_{0.9}RuO_6$ measured in 1 kG.

the measured temperature range is not allowed by the proposed structure and, given that no additional peaks were observed in the data collected on HRPD at 4.5 K, we believe that it is an instrumental effect.

DISCUSSION

The coexistence of Cu^{2+} and Ca^{2+} on the prismatic site of a K_4CdCl_6 material has been reported previously (18). In that case ($Ca_{1.75}Sr_{1.5}Cu_{0.75}PtO_6$) the Ca^{2+} cation remained at the center of the prism and the Cu^{2+} cations were displaced toward the rectangular faces of the prisms in a disordered manner. The structure thus adopted the rhombohedral space group $R\bar{3}c$, as do the majority of $A_3A'BO_6$ phases. However, the presence of a higher concentration of Jahn–Teller active Cu^{2+} in $Ca_{3.1}Cu_{0.9}RuO_6$ causes an ordering of the displacements and hence a reduction of the space group symmetry to monoclinic $C2/c$. As a consequence of the displacements, the Cu^{2+} cations adopt a pseudo-square-planar coordination. This effect has previously been observed in the K_4CdCl_6 phases Ca_3CuIrO_6, Sr_3CuIrO_6, and Sr_3CuPtO_6. A comparison of the environment of the Cu in the trigonal prisms of $Ca_{3.1}Cu_{0.9}RuO_6$ to those found in the other compounds shows that the four

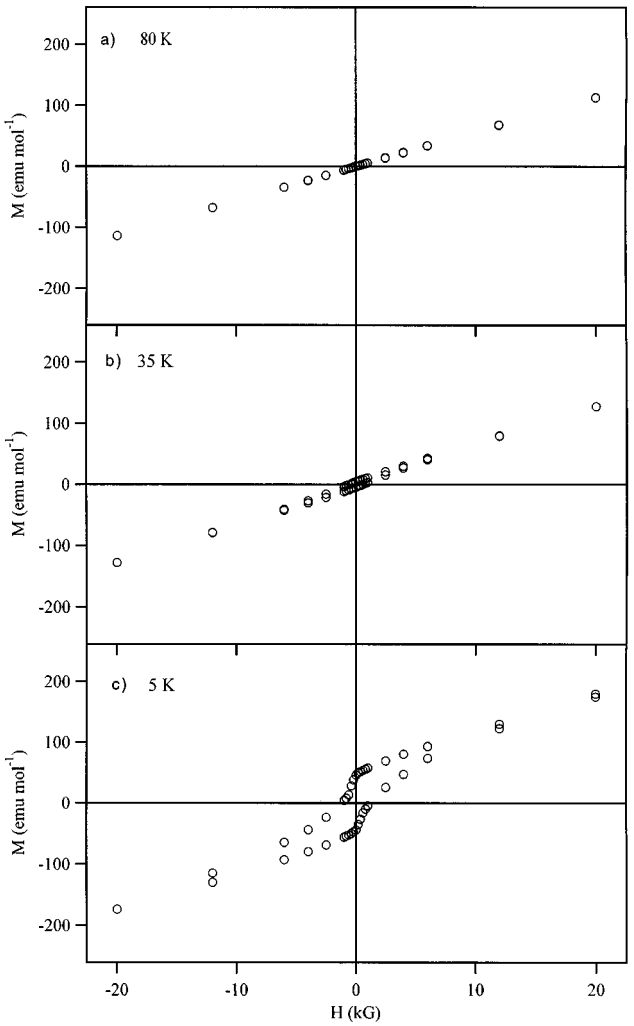

FIG. 5. Field dependence of the molar magnetization of $Ca_{3.1}Cu_{0.9}RuO_6$ measured at (a) 80, (b) 35, and (c) 5 K.

short Cu–O distances are all essentially equal in each case, as they are in the structurally related phase $Ba_6Mn_4CuO_{15}$ (14). In the latter case, the Cu/Mn disorder in the prismatic sites (67:33) is sufficient to quench any cooperative transition to monoclinic symmetry and the cation displacements are disordered. The presence of 10% Ca in these sites is clearly insufficient to prevent an ordered displacement in $Ca_{3.1}Cu_{0.9}RuO_6$. Our refinements assumed that only one cation site exists within the prisms, and therefore that the Ca cations are also displaced away from the center. However, the temperature factor of the Cu/Ca cation is large at both room temperature and 5 K ($U_{iso} = 0.0107(6)$ Å^2), an indication that the elements are disordered over two or more unresolved positions.

Ca_3NaRuO_6 and Ca_3LiRuO_6 are the only Ca/Ru-containing K_4CdCl_6 phases to have been studied by neutron diffraction. These compounds contain Ru^{5+}, rather than Ru^{4+}, as in $Ca_{3.1}Cu_{0.9}RuO_6$, and the newly prepared phase therefore facilitates a study of the effect of reducing Ru in this type of compound. The mean length of a Ru–O bond in $Ca_{3.1}Cu_{0.9}RuO_6$ is, predictably, slightly longer than that in either Ca_3NaRuO_6 or Ca_3LiRuO_6. The bond lengths reported for the Ru^{5+} phases indicate that they contain regular RuO_6 octahedra, which is to be expected for a $4d^3$:Ru^{5+} ion with a $^4A_{2g}$ ground state. The Ru–O bond lengths calculated for $Ca_{3.1}Cu_{0.9}RuO_6$ show clearly that there are four essentially equal Ru–O bonds and two significantly shorter bonds. This distortion can be attributed to the displacement of the Cu^{2+} cations; the two oxygen atoms (O3) that are furthest from the Cu in the trigonal prisms move closer to the Ru in the octahedra to compensate, hence distorting the shape of the octahedron. The O1–O2 separation along the common edge of the octahedron and the CuO_4 rectangle is the shortest anion–anion contact in the structure, and the angle subtended by this pair at the Ru cation is decreased to 84.6°. We note that the shortening of two *trans* bonds (Ru–O3) in an octahedron coordinating a d^4 cation is expected to quench the orbital contribution to the magnetic moment of that cation. The distortion of the IrO_6 octahedra in Ca_3CuIrO_6 is much less pronounced than that of the RuO_6 octahedra in $Ca_{3.1}Cu_{0.9}RuO_6$.

The parameters derived from our magnetometry data indicate that $Ca_{3.1}Cu_{0.9}RuO_6$ does not behave as a simple paramagnet, even at relatively high temperatures (>150 K). The observation of both a high Curie constant (much greater than the value of 1.34 emu expected for the relevant concentrations of Cu^{2+} and Ru^{4+}) and an unusually high value for the ratio θ/T_N shows that the Curie–Weiss Law cannot be used to account for the behavior of this material. The high value of the fitted Curie constant is a consequence of the relatively low rate of increase of the susceptibility with decreasing temperature. Given the one-dimensional nature of the structure, a plausible explanation for this behavior is that in the high-temperature region short-range antiferromagnetic coupling persists within the individual chains and that the magnetic transition at $\sim$50 K is associated with the onset of three-dimensional magnetic ordering between one-dimensional ordered systems. Similar arguments have been used (14) to explain the behavior of $Ba_6Mn_4CuO_{15}$ and the partly diluted analogue $Ba_6Mn_4ZnO_{15}$, the magnetic susceptibilities of which could not be interpreted in terms of Curie–Weiss behavior in any part of the temperature range $5 \leq T/K \leq 300$. In dilute Ca_3LiRuO_6 the susceptibility data were typical of a Curie–Weiss paramagnet undergoing a transition to an antiferromagnetic state. This compound has Li in the trigonal prismatic sites; hence, the distances between neighboring paramagnetic species within a single chain are comparable to those between chains, and the magnetic interactions within chains and between chains are of approximately the same magnitude. In contrast to the case of the more concentrated materials, the Néel temperature of

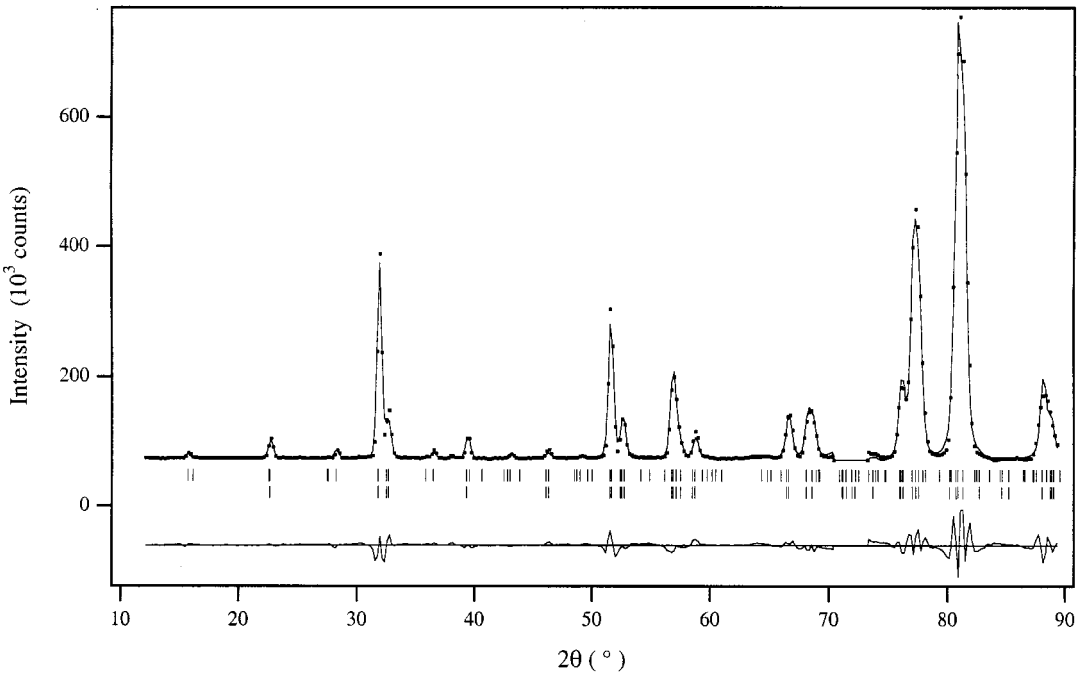

FIG. 6. Observed, calculated, and difference neutron diffraction profiles of $Ca_{3.1}Cu_{0.9}RuO_6$ at 3.7 K. Reflection positions are marked for the magnetic (upper) and crystallographic (lower) structures. A region of strong instrumental scattering at $2\theta \sim 72^\circ$ was excluded from the refinement.

the dilute compound thus corresponds to a transition between paramagnetism and three-dimensional magnetic ordering. However, detailed consideration of the behavior of $Ba_6Mn_4CuO_{15}$ and $Ba_6Mn_4ZnO_{15}$ shows that this simple argument is incomplete. The Cu^{2+} cations in the former have been shown to be paramagnetic down to the Néel temperature and, consistent with the presence of nonmagnetic Zn^{2+} in the latter, this suggests that the short-range

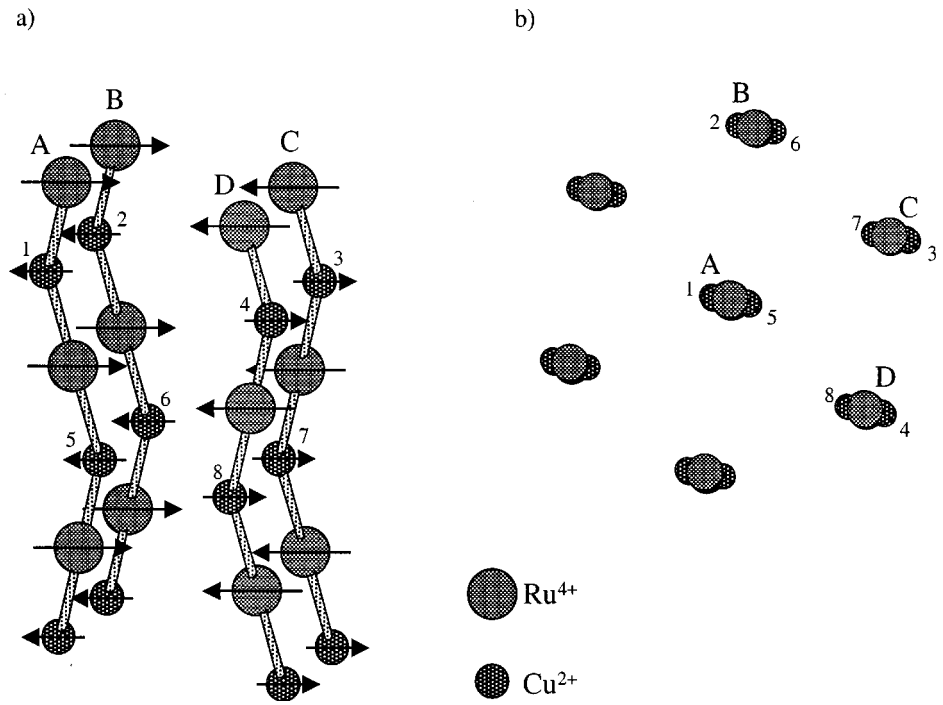

FIG. 7. (a) Magnetic structure of the transition metal sublattice of $Ca_{3.1}Cu_{0.9}RuO_6$, viewed perpendicular to the polyhedral chains and (b) view along the chains emphasizing the symmetry lowering caused by displacement of Cu^{2+}.

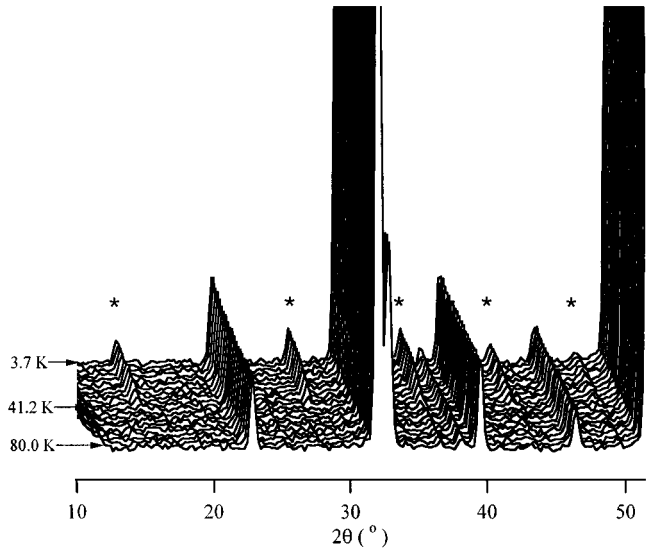

FIG. 8. Observed neutron diffraction pattern of $Ca_{3.1}Cu_{0.9}RuO_6$ as a function of temperature in the range $3.7 \leq T/K \leq 80$. Magnetic reflections are marked (*).

magnetic order in these compounds involves the octahedral sites but not the prismatic site. $Ca_{3.1}Cu_{0.9}RuO_6$ is thus unusual within this structural family in that the cation in the prismatic site is involved in the formation of one-dimensional ordered chains. This may be facilitated by the presence of an ordered distribution of paramagnetic cations on that site, in contrast to the situation in the Zn (diamagnetic) and Cu (disordered) compounds.

The saturation values determined for the ordered moments on the Ru^{4+} and Cu^{2+} cations (1.1(1) μ_B per Ru and 0.5(1) μ_B per Cu) are comparable to those observed previously for the same species, for example, 1.3 μ_B per Ru^{4+} in Ca_2RuO_4 (19), 0.5 μ_B per Cu^{2+} in La_2CuO_4 (20), and 0.48(3) μ_B per Cu^{2+} in Pr_2CuO_4 (21). The reduction from the spin-only values is no greater than that to be expected because of covalent effects, and it appears that the dilution of the prismatic sites with diamagnetic Ca^{2+} does not unduly influence the magnetic properties of the compound. The magnetic structure adopted by $Ca_{3.1}Cu_{0.9}RuO_6$ can be understood by considering the distances between the magnetic cations while making the assumption that all the cation–cation interactions are inherently antiferromagnetic. The strongest interaction is obviously that between Cu^{2+} and Ru^{4+} in neighboring, face-sharing polyhedra within an individual chain. This leads to the formation of ferrimagnetic chains as discussed above. In the absence of the monoclinic distortion, the distances between like cations in neighboring chains would all be equal, the magnetic ground state would be degenerate, and frustration might be expected to lead to the adoption of a noncollinear spin structure. The interchain Ru–Ru distance remains constant (5.62 Å) despite the symmetry lowering but the displacements of the Cu^{2+} cations, which cause the reduction in symmetry, eliminate the degeneracy and allow the formation of a nonfrustrated antiferromagnetic state. As can be seen from Fig. 7, the displacements lead to distortions of the chains, pairs of which can consequently be described as "in-phase," for example, chains A and B or C and D, or "out-of-phase," for example, chains A and D or A and C. The Cu–Cu distance between in-phase chains is constant (5.72 Å), whereas that between cations in out-of-phase chains is either shortened (4.79 Å) or lengthened (6.57 Å). The magnetic structure adopted is that which renders all the short Cu–Cu interactions antiferromagnetic, although it should be recognized that the interaction is actually by superexchange (involving oxide ions) rather than by direct exchange. Magnetic structures for other low-dimensional compounds consisting of chains of octahedra and trigonal prisms have been reported previously (11, 13). As described above, the nonfrustrated magnetic structures of Ca_3NaRuO_6 and Ca_3ZnMnO_6 have the magnetic cations ordered antiferromagnetically within the chains, and the moments on nearest neighbor Ru or Mn ions in adjacent chains align in a collinear antiferromagnetic manner. However, Ca_3NiMnO_6, in which the occupation of the prismatic sites by a paramagnetic cation introduces frustration that is not eliminated by a structural distortion, adopts a noncollinear, 120° spin arrangement. This emphasizes the importance of the crystal structure, and in particular the symmetry lowering, in determining the magnetic structure of $Ca_{3.1}Cu_{0.9}RuO_6$.

In summary, the results described above demonstrate that Ru^{4+} and Cu^{2+} can coexist in the K_4CdCl_6 structure, albeit over a relatively (22) narrow composition range. The high Néel temperatures observed in analogous Ru^{5+} compounds are not reproduced, but long-range magnetic order is achieved at 42 K. Although the low-temperature phase is weakly ferromagnetic, the spontaneous magnetization is too small to be detected by neutron diffraction and the magnetic structure can reasonably be approximated by a collinear-spin antiferromagnetic model. The Jahn–Teller distortion brought about by the presence of Cu^{2+} results in a magnetic structure that is very different from those observed in analogous Ni and Zn compounds.

ACKNOWLEDGMENTS

We are grateful to EPSRC for financial support and the provision of neutron diffraction facilities at ILL Grenoble, where Thomas Hansen provided experimental assistance, and at RAL, where we were helped by Richard Ibberson. We had interesting discussions with Jacques Darriet and Fabien Grasset (ICMCB Bordeaux).

REFERENCES

1. G. Bergerhoff and O. Schimtz-Dumont, *Z. Anorg. Allg. Chem.* **284,** 10 (1956).

2. T. N. Nguyen and H.-C. zur Loye, *J. Solid State Chem.* **117,** 300 (1995).
3. P. Nunez, S. Trail, and H.-C. zur Loye, *J. Solid State Chem.* **130,** (1997).
4. M. Neubacher and H. Müller-Buschbaum, *Z. Anorg. Allg. Chem.* **607,** 124 (1992).
5. A. Tomaszewska and H. Müller-Buschbaum, *Z. Anorg. Allg. Chem.* **619,** 534 (1993).
6. J. L. Hodeau, H. Y. Tu, P. Bordet, T. Fournier, P. Strobel, and M. Marezio, *Acta Crystallogr. B* **48,** 1 (1992).
7. A. P. Wilkinson, A. K. Cheetham, W. Kunnman, and Kvick, *Eur. J. Solid State Chem.* **28,** 453 (1991).
8. C. Lampe-Önnerud and H.-C. zur Loye, *Inorg. Chem.* **35,** 2155 (1996).
9. N. Segal, J. F. Vente, T. S. Bush, and P. D. Battle, *J. Mater. Chem.* **6,** 395 (1996).
10. J. F. Vente, J. K. Lear, and P. D. Battle, *J. Mater. Chem.* **5,** 1785 (1995).
11. P. D. Battle, G. R. Blake, J. C. Burley, E. J. Cussen, J. Sloan, J. F. Vente, J. Darriet, and F. Weill, *Mater. Res. Soc. Symp. Proc.* **547,** 45 (1999).
12. J. Darriet, F. Grasset, and P. D. Battle, *Mater. Res. Bull.* **32,** 139 (1997).
13. S. Kawasaki, M. Takano, and T. Inami, *J. Solid State Chem.* **145,** 302 (1999).
14. E. J. Cussen, J. F. Vente, ad P. D. Battle, *J. Am. Chem. Soc.* **121,** 3958 (1999).
15. H. W. Zandbergen, *J. Solid State Chem.* **35,** 367 (1980).
16. H. M. Rietveld, *J. Appl. Crystallogr.* **2,** 65 (1969).
17. A. C. Larson and R. B. von-Dreele, "General Structure Analysis System (GSAS)." Report LAUR 86-748. Los Alamos National Laboratories, Los Alamos, NM, 1990.
18. A. B. Bykov, S. F. Radaev, E. A. Genkina, L. N. Dem'yanets, B. A. Makisimov, and O. K. Mel'nikov, *Sov. Phys. Crystallogr.* **35,** 511 (1990).
19. M. Braden, G. André, S. Nakatsuji, and Y. Maeno, *Phys. Rev. B* **58,** 847 (1998).
20. D. Vaknin, S. K. Sinha, D. E. Moncton, D. C. Johnston, J. M. Newsam, C. R. Safinya, and H. E. King, *Phys. Rev. Lett.* **58,** 2802 (1987).
21. D. E. Cox, A. I. Goldman, M. A. Subramanian, J. Gopalkrishnan, and A. W. Sleight, *Phys. Rev. B* **40,** 6998 (1989).
22. H. Kageyama, K. Yoshimura, and K. Kosuge, *J. Solid State Chem.* **140,** 14 (1998).